ARTICLE   OPEN

Orbital-selective pairing and superconductivity in iron selenides

Emilian M. Nica[1], Rong Yu[2] and Qimiao Si[3]

An important challenge in condensed matter physics is understanding iron-based superconductors. Among these systems, the iron selenides hold the record for highest superconducting transition temperature and pose especially striking puzzles regarding the nature of superconductivity. The pairing state of the alkaline iron selenides appears to be of d-wave type based on the observation of a resonance mode in neutron scattering, while it seems to be of s-wave type from the nodeless gaps observed everywhere on the Fermi surface. Here we propose an orbital-selective pairing state, dubbed $s\tau_3$, as a natural explanation of these disparate properties. The pairing function, containing a matrix τ_3 in the basis of $3d$-electron orbitals, does not commute with the kinetic part of the Hamiltonian. This dictates the existence of both intraband and interband pairing terms in the band basis. A spin resonance arises from a d-wave-type sign change in the intraband pairing component, whereas the quasiparticle excitation is fully gapped on the FS due to an s-wave-like form factor associated with the addition in quadrature of the intraband and interband pairing terms. We demonstrate that this pairing state is energetically favored when the electron correlation effects are orbitally selective. More generally, our results illustrate how the multiband nature of correlated electrons affords unusual types of superconducting states, thereby shedding new light not only on the iron-based materials but also on a broad range of other unconventional superconductors such as heavy fermion and organic systems.

INTRODUCTION

Unconventional superconductivity is driven by electron–electron interactions, instead of electron–phonon couplings.[1] It occurs in a variety of strongly correlated electron systems, with the iron-based superconductors (FeSCs) representing a prototype case.[2–7] The field of FeSC started with most of the efforts being directed toward the iron pnictide class. The normal state was found to be a bad metal, with room-temperature resistivity reaching the Mott-Ioffe-Regel limit,[3, 8] suggesting the importance of electron correlations.[9, 10] More recently, the focus has been shifted to iron selenide systems. The reasons are manifold. They have the highest T_c,[11, 12] they show even stronger electron correlations, and, as we discuss here, their superconductivity is highly unusual.

The puzzle of the superconducting pairing state is highlighted by the "122" alkaline iron selenides. These systems have a T_c of ~31 K at ambient pressure. They have only electron Fermi pockets, lacking the hole pockets that exist in the iron pnictides at the center of the Brillouin zone (BZ).[13–15] Angle-resolved photoemission spectroscopy (ARPES) experiments show that the quasiparticle dispersion is fully gapped on all the parts of the Fermi surface (FS),[13–15] including a small electron Fermi pocket at the center of the BZ.[16, 17] This is compatible with the usual s-wave A_{1g} pairing state, but not with the usual d-wave B_{1g} state (which would produce nodes on the small electron Fermi pocket near the center of the BZ). On the other hand, inelastic neutron scattering experiments[18, 19] observe a sharp resonance peak around the wavevector $(\pi, \pi/2)$. It is consistent with a pairing function that changes sign[20] between the two Fermi pockets at the edge of the

BZ, such as would occur in a d-wave B_{1g} state, but not in the usual s-wave A_{1g} case.

In this work, we demonstrate how an orbital-selective pairing state, dubbed $s\tau_3$, exhibits properties that are commonly associated with a d-wave B_{1g} state or a s-wave A_{1g} state. The key to the emergence of this superconducting state is the multiband nature of the FeSCs. This is associated with the multiplicity of $3d$ electron orbitals, whose conceptual importance follows the tradition wherein new physics develops out of extra degrees of freedom, similar, for instance, to the way the so-called valley quantum number in the electronic structure introduces new topological properties.[21] It is important for the FeSCs that there are multiple orbitals at play in the neighborhood of the Fermi level. Thus, there is reason to expect that correlation effects will be different for different orbitals. In fact, there is evidence for orbitally selective Mott behavior in the iron selenides[22–26] and, thus, orbital selectivity is to be expected for pairing as well.

For strongly correlated superconductivity, Cooper pairing is naturally considered in an orbital basis due to the tendency of the electrons to avoid the dominating Coulomb repulsions. Considering a basis formed from all five $3d$ orbitals, the $s\tau_3$ state has an s-wave form factor, but transforms as a d-wave B_{1g} state. As such, it represents an energetically favored reconstruction of the conventional s-wave and d-wave pairing states when they are quasi-degenerate, due to frustrated antiferromagnetic interactions.[27] The pairing function incorporates a matrix τ_3 in the $3d_{xz}$, $3d_{yz}$ subspace, which does not commute with the kinetic term of the Hamiltonian. Consequently, in the band basis, it must also have a matrix structure, which contains both intraband and interband

[1]Department of Physics and Astronomy and Quantum Materials Institute, University of British Columbia, Vancouver, BC V6T 1Z1, Canada; [2]Department of Physics, Renmin University of China, 59 Zhongguancun St, Beijing 100872, China and [3]Department of Physics and Astronomy, Rice University, 6100 Main St, Houston 77005 TX, USA
Correspondence: Emilian M. Nica (enica@qmi.ubc.ca) or Qimiao Si (qmsi@rice.edu)

terms. This allows the intraband pairing component to have a d-wave sign change, while the addition in quadrature of the intraband and interband pairing terms is nonzero everywhere on the FS. Thereby, the spin excitations show a $(\pi, \pi/2)$ resonance, while the quasiparticle excitations as measured by ARPES are fully gapped on the FS.

RESULTS

Orbital selectivity in the normal state of iron selenides

In the normal state, ARPES has provided evidence not only for the existence of the orbital degree of freedom but also for the strong orbital-selective correlation effects on the iron selenides. These materials include the alkaline iron selenides, the Te-doped "11" iron selenides FeSe, and the monolayer FeSe on the SrTiO$_3$ substrate.[22–26] The effective quasiparticle mass normalized by its non-interacting counterpart, m^*/m_{band} is on the order of 3–4 for the $3d_{yz,yz}$ orbitals, but is as large as 20 for the $3d_{xy}$ orbital.[22, 23, 28] Such orbital selectivity has also been the subject of extensive recent theoretical studies.[29–31] All these aspects make it natural to study orbital-dependent[32–34] and -related[35] superconducting pairing. We are thus motivated to address the hitherto unexplored question, viz. whether there exists an orbital-selective pairing state that can reconcile the seemingly contradictory properties observed in the iron selenide superconductors. We also examine the stability of such a pairing state at the level of an effective Hamiltonian for studying superconductivity, in which we incorporate the orbital selectivity in the short-range exchange interactions (see Supplementary Information).

Orbital-selective $s\tau_3$ pairing state—a simplified case

We first discuss the structure and properties of the $s\tau_3$ pairing state in a simplified two-orbital d_{xz}, d_{yz} system. This illustrates how features typically associated with both standard structure-less s- and d-wave states can simultaneously arise. The salient features of the two-orbital model are illustrated in Fig. 1.

We consider spin-singlet pairing in the orbital basis, in the case of two orbitals $3d_{xz}$, $3d_{yz}$.[36] The Hamiltonian, incorporating the $s\tau_3$ pairing term, is given by

$$\hat{H} = \sum_{\boldsymbol{k}} \psi_{\boldsymbol{k}}^{\dagger} \left(\hat{H}_{\text{Kinetic}}(\boldsymbol{k}) + \hat{H}_{\text{Pair}}(\boldsymbol{k}) \right) \psi_{\boldsymbol{k}}$$

$$\hat{H}_{\text{Kinetic}} = \left(\xi_+(\boldsymbol{k}) \otimes \tau_0 + \xi_-(\boldsymbol{k}) \otimes \tau_3 + \xi_{xy}(\boldsymbol{k}) \otimes \tau_1 \right) \otimes \sigma_0 \otimes \gamma_3$$

$$\hat{H}_{\text{Pair}} = \Delta_0 g_{x^2y^2}(\boldsymbol{k}) \otimes \tau_3 \otimes \sigma_0 \otimes \gamma_1,$$

(1)

where $\psi_{\boldsymbol{k}}^{\dagger} = (c_{\boldsymbol{k}i\sigma}^{\dagger}, c_{-\boldsymbol{k}j\sigma'}(i\sigma_2)_{\sigma'\sigma})$ is equivalent to a Nambu spinor, and i and j are orbital indices (Supplementary Information). The τ_i, σ_i and γ_i ($i = 0, \ldots, 4$) 2×2 Pauli matrices represent orbital iso-spin, spin, and Nambu indices, respectively. The ξ_+, ξ_-, and ξ_{xy} factors appearing in the kinetic part belong to the A_{1g}, B_{1g}, and B_{2g} irreducible representations of the D_{4h} point-group. Their exact forms, as well as the resulting electron bands, are given in Supplementary Information.

The even-parity, spin-singlet candidate $s\tau_3$ pairing function with non-trivial orbital structure is included in the $\hat{H}_{\text{Pair}}$ term in Eq. 1. While Δ_0 is a (generally) complex number, we choose a real amplitude for convenience. The form factor $g_{x^2y^2}(\boldsymbol{k})$ is parity-even and belongs to the A_{1g} representation of the D_{4h} point-group. In the absence of spin–orbit coupling, the rotational properties of the $s\tau_3$ pairing are of B_{1g} symmetry. The latter is entirely determined by the tensor product of the $g_{x^2y^2}(\boldsymbol{k})$ (s-wave) form factor and the τ_3 orbital matrix. To illustrate, under a C_{4z} rotation, the form-factor is invariant, while the τ_3 matrix transforms as a
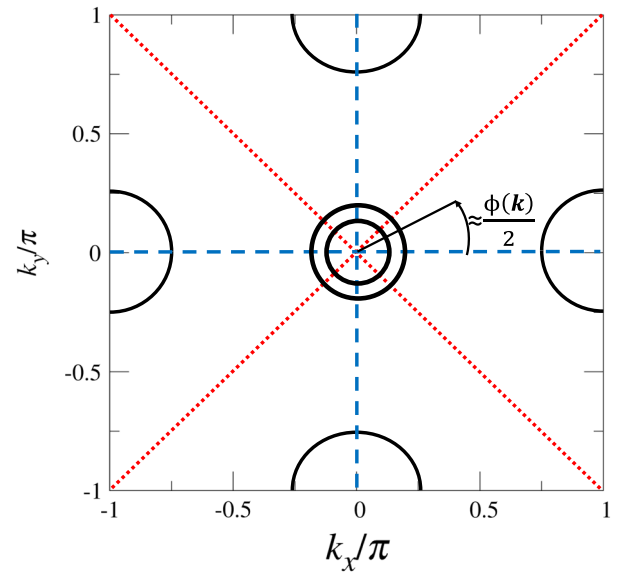

Fig. 1 Schematic illustration of the two-orbital $s\tau_3$ pairing in a 1-Fe Brillouin zone (BZ), which is obtained by unfolding the 2D crystallographic BZ cell in the conventional manner.[55] The *solid lines* indicate typical Fermi pockets for the Fe-based superconductors. The *dotted, red lines* indicate the zeroes specific to the intraband pairing (ξ_-), while the *dashed, blue lines* mark the zeroes specific to the interband pairing (ξ_{xy}). The intra- and interband components do not vanish at the same subset of $\boldsymbol{k}$, ensuring that there is always a non-zero pairing given by either of the two components on the entire Fermi surface. For $\max(\xi_-) \approx \max(\xi_{xy})$ the angle $\phi(\boldsymbol{k})$ (Eqs 5–7) can be roughly identified with twice the winding angle shown for fixed $|\boldsymbol{k}|$. In addition, there is a sign change between the intraband pairing along the two pockets at the edge of the BZ, a condition necessary to the formation of a resonance in the spin-excitation spectrum at the wavevector $\boldsymbol{q} = (\pi, \pi/2)$ observed in experiment.[50]

rank-two B_{1g} tensor representation of the point-group, i.e., it changes sign. We note that the anti-symmetry under exchange is guaranteed by the spin-singlet nature, together with the even-parity of the form factor. Since the spin-structure is not essential for the following arguments, we shall henceforth omit the explicit σ_0 matrix.

The non-trivial characteristics of this pairing are consequences of the commutator $\left[\hat{H}_{\text{Kinetic}}, \hat{H}_{\text{Pair}} \right] \neq 0$ for general momentum $\boldsymbol{k}$. We use the notation of ref. 34, and rewrite the Hamiltonian Eq. 1 as follows:

$$\hat{H} = \sum_{\boldsymbol{k}} \psi^{\dagger}(\boldsymbol{k}) \left[\left(\xi_+(\boldsymbol{k}) \tau_0 + \vec{B}(\boldsymbol{k}) \cdot \vec{\tau} \right) \otimes \gamma_3 \right. $$
$$\left. + \left(\vec{d}(\boldsymbol{k}) \cdot \vec{\tau} \right) \otimes \gamma_1 \right] \psi(\boldsymbol{k}),$$

(2)

where

$$\vec{B}(\boldsymbol{k}) = (\xi_{xy}(\boldsymbol{k}), 0, \xi_-(\boldsymbol{k}))$$
$$\vec{d}(\boldsymbol{k}) = (0, 0, \Delta_0 g_{x^2y^2}(\boldsymbol{k})).$$

(3)

This is formally similar to a Balian–Werthamer form[37–39] (see Supplementary Information for more details), with the $\vec{B}(\boldsymbol{k})$ factor being analogous to a $\boldsymbol{k}$-dependent spin–orbit coupling. To account for the non-commuting $\hat{H}_{\text{Kinetic}}$ and $\hat{H}_{\text{Pair}}$, we write the

square of the Hamiltonian matrix as follows:

$$\hat{H}^2 = \sum_{\boldsymbol{k}} \left[\xi_+(\boldsymbol{k})\tau_0 + \left(\vec{B}_{\boldsymbol{k}} \cdot \vec{\tau}\right) \right]^2 \otimes \gamma_0 + \left| \vec{d}(\boldsymbol{k}) \right|^2 \tau_0 \otimes \gamma_0 \tag{4}$$
$$+2i\left(\vec{B}(\boldsymbol{k}) \times \vec{d}(\boldsymbol{k})\right) \cdot \vec{\tau} \otimes i\gamma_2.$$

where the well-known relation $(\vec{a} \cdot \vec{\tau})(\vec{b} \cdot \vec{\tau}) = \vec{a} \cdot \vec{b} + i(\vec{a} \times \vec{b}) \cdot \vec{\tau}$ was used. The first two terms, proportional to the γ_0 Nambu matrix, are the squares of the kinetic Hamiltonian and of a pairing contribution with no essential structure in orbital space, given by $\left| \vec{d}(\boldsymbol{k}) \right|^2$. The latter is an effective amplitude of the pairing interactions and, as such, is proportional to the square of the s-wave-like $g_{x^2y^2}$ form factor, as can be seen from Eq. 3. Together with the kinetic part, it amounts to the usual (and sole) contribution to the Bogoliubov–de Gennes (BdG) quasiparticle spectrum, whenever $[\hat{H}_{\text{Kinetic}}, \hat{H}_{\text{Pair}}] = 0$ for all $\boldsymbol{k}$. The last term in Eq. 4 reflects the non-commuting $\hat{H}_{\text{Kinetic}}$ and $\hat{H}_{\text{Pair}}$. Since the Nambu matrices γ_0 and $i\gamma_2$ commute, $\hat{H}^2$ in Eq. 4 can be easily expressed in block diagonal form (Supplementary Information). The resulting BdG bands are given by

$$E_\pm(\boldsymbol{k}) =$$
$$\sqrt{\left(\sqrt{\xi_+^2(\boldsymbol{k}) + \left| \vec{d}(\boldsymbol{k}) \right|^2 \sin^2\phi(\boldsymbol{k})} \pm \left| \vec{B}(\boldsymbol{k}) \right| \right)^2 + \left| \vec{d}(\boldsymbol{k}) \right|^2 (1 - \sin^2\phi(\boldsymbol{k}))}, \tag{5}$$

where

$$\sin\phi(\boldsymbol{k}) = \frac{\xi_{xy}(\boldsymbol{k})}{\left| \vec{B}(\boldsymbol{k}) \right|} = \frac{\xi_{xy}(\boldsymbol{k})}{\sqrt{\xi_-^2(\boldsymbol{k}) + \xi_{xy}^2(\boldsymbol{k})}}. \tag{6}$$

The terms proportional to $\sin\phi(\boldsymbol{k})$ reflects the non-Abelian aspect of the pairing state. Note that Eq. 5 corresponds to the sum of two positive semi-definite terms. For general $\vec{d}(\boldsymbol{k})$, we see that nodes can appear only when both terms in the square root vanish. The second of these goes to zero when either $\sin\phi(\boldsymbol{k}) = 1$ or, trivially, when $\left| \vec{d}(\boldsymbol{k}) \right| = 0$. This latter case occurs when the FS intersects the lines of zeros of the $g_{x^2y^2}$ form factor. With the FeSCs in mind, we ignore this simple case in the following. Alternately, when $\sin\phi(\boldsymbol{k}) = 1$, the dispersion reduces to

$$E_\pm(\boldsymbol{k}) = \left| \sqrt{\xi_+^2(\boldsymbol{k}) + \left| \vec{d}(\boldsymbol{k}) \right|^2} \pm \left| \vec{B}(\boldsymbol{k}) \right| \right|. \tag{7}$$

On the FS, we have $\xi_+^2(\boldsymbol{k}) = \left| \vec{B}(\boldsymbol{k}) \right|^2$ (see Supplementary Information). Thus, there are no nodes on the FS.

We note that away from the FS, Eq. 7 does not in general guarantee the absence of nodes. However, because the lifetime of quasiparticles away from the FS will be finite, the corresponding contributions to thermodynamic properties will be much weaker compared to the case of nodes on the FS.

In the band basis, the kinetic part of the Hamiltonian is diagonalized. Given that the kinetic and pairing parts do not commute with each other, the two cannot be simultaneously diagonalized. Thus, the pairing part must contain an interband component. To see this, we apply a canonical transformation that diagonalizes the kinetic part (see Supplementary Information), but which also transforms the pairing into

$$\hat{H}_{\text{Pair}}(\boldsymbol{k}) = \Delta_1(\boldsymbol{k})\alpha_3 + \Delta_2(\boldsymbol{k})\alpha_1, \tag{8}$$

where α_1 and α_3 are Pauli matrices corresponding to inter- and intraband pairing terms, respectively. The two components are

given by

$$\Delta_1(\boldsymbol{k}) = -\Delta_0 g_{x^2y^2}(\boldsymbol{k}) \frac{\xi_-(\boldsymbol{k})}{\sqrt{\xi_-^2(\boldsymbol{k}) + \xi_{xy}^2(\boldsymbol{k})}}$$
$$\Delta_2(\boldsymbol{k}) = -\Delta_0 g_{x^2y^2}(\boldsymbol{k}) \frac{\xi_{xy}(\boldsymbol{k})}{\sqrt{\xi_-^2(\boldsymbol{k}) + \xi_{xy}^2(\boldsymbol{k})}}. \tag{9}$$

The band-diagonal α_3 and band off-diagonal α_1 pairing components have $d(x^2-y^2)$ and $d(xy)$ form factors, respectively. As illustrated in Fig. 1, these have nodes along the diagonals and axes of the BZ, respectively. Because the two matrices α_1 and α_3 anti-commute, the single-particle excitation energy depends on the addition in quadrature of the two pairing amplitudes $\Delta_1(\boldsymbol{k})$ and $\Delta_2(\boldsymbol{k})$. This ensures that the excitation gap is nodeless on the entire FS.

As can be seen from Eqs 8 and 9, the band-index diagonal term changes sign about the diagonals ($k_x = \pm k_y$) of the BZ, as dictated by the $d(x^2-y^2)$ nature of the intraband component. Thus, the intraband pairing component does indeed change sign between the two-electron Fermi pockets at the BZ boundaries. It ensures that this type of pairing is conducive to the formation of a resonance with a wavevector that connects the two-electron Fermi pockets.

We stress that the two main features of the $s\tau_3$ pairing, i.e., the formation of a gap on the FS and the sign change in the intraband component, cannot be reconciled by the more typical pairing candidates, which lack an orbital structure. In the context of our two-orbital model, the $s\otimes\tau_0$ and $d\otimes\tau_0$ candidate states, corresponding to the typical orbitally trivial s- and d-wave pairings, commute with $\hat{H}_{\text{Kinetic}}$. Consequently, they are associated with intraband pairing only. As such, neither of the two types can induce a nodeless gap and account for the sign change required for the spin-resonance.

Orbital-selective $s\tau_3$ pairing state—the case of iron selenides

Superconductivity in the alkaline iron selenides, like in the related case of the iron pnictides, involves all five Fe 3d-orbitals. Thus, it is important to consider the five-orbital case to address (i) whether the $s\tau_3$ pairing state is energetically favored compared to the more conventional pairing states and (ii) whether it captures the essential properties of this pairing state as they pertain to the iron selenide superconductors.

To study the stability of the $s\tau_3$ pairing state, we start from two previously discussed aspects of the FeSCs. We do so in terms of a strong-coupling approach to superconductivity, in light of the strong correlation effects[9, 10, 31, 40–48] that are especially clear-cut for the iron selenides.[22, 23, 28] This approach is described in Supplementary Information, with superconductivity driven by short-range interactions. The latter include the antiferromagnetic interactions between the nearest-neighbor (J_1^a) and next-nearest-neighbor (J_2^a) Fe sites on their square lattice, for the three most relevant orbitals, $a = 3d_{xz}$, $3d_{yz}$, and $3d_{xy}$. We reiterate that we will analyze the model in the 1-Fe unit cell and the corresponding BZ.

One of the known aspects of the FeSCs is the large parameter regime where the conventional d-wave B_{1g} and s-wave A_{1g} pairing states are quasi-degenerate.[27, 49] In terms of a model with short-range antiferromagnetic interactions, this occurs in the regime of magnetic frustration with J_2 being comparable to J_1,[27] a condition that is evidenced by both theoretical considerations and experimental measurements.[4, 50] To quantify this effect, we introduce the ratio $A_L \equiv J_2/J_1$ to describe the relative strength of these two interactions. For a proof-of-concept demonstration, we analyze the phase diagram by taking the J_2/J_1 axis to be a cut in the parameter space along which A_L is the same for the different 3d-orbitals. The quasi-degeneracy arises when $A_L \sim 1$.
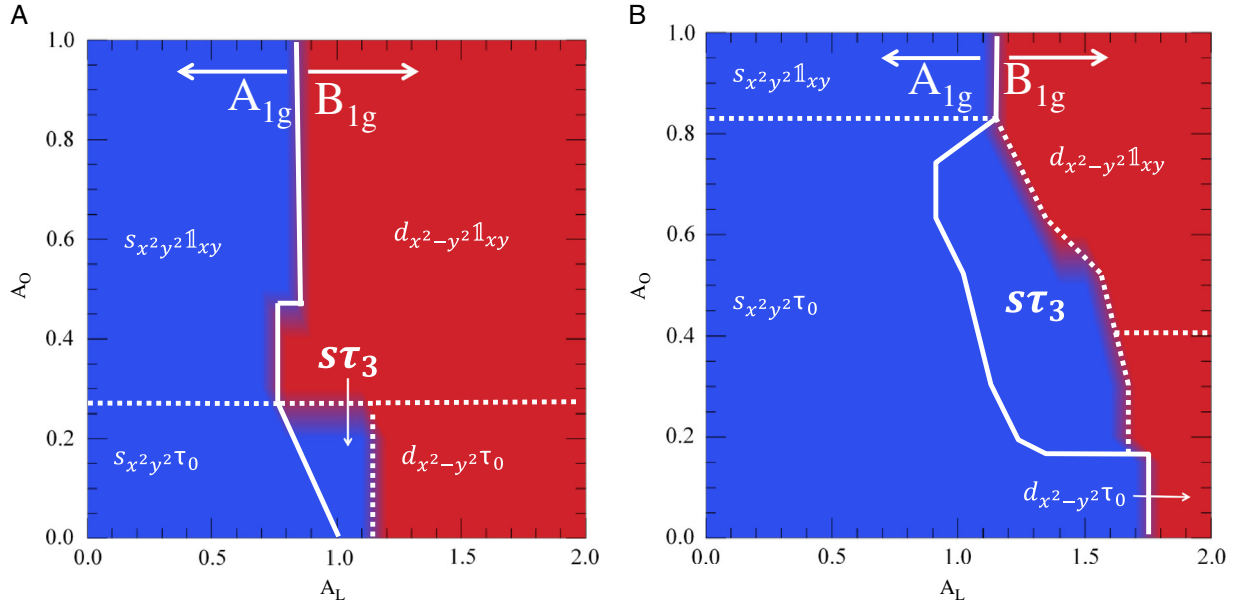
A

B

Fig. 2 Phase diagrams based on the leading pairing amplitudes given by self-consistent calculations with fixed $J_2 = 1$ and tight-binding parameters appropriate to **a** alkaline iron selenides and **b** iron pnictides. The tight-binding parameters used can be found in ref. [27]. The *blue shaded areas* correspond to dominant pairing channels with an $s_{x^2y^2}$ form factor, while the *red shading covers* those with a $d_{x^2-y^2}$ form factor. The *continuous line* separates regions where the pairing belongs to the A_{1g} and the B_{1g} representations, respectively. The 1×1 matrix in the d_{xy} subspace is represented by 1_{xy}. The orbital-selective $s\tau_3$ pairing occurs for $A_O < 1$, A_L near 1 in all cases

The second well-known property of the FeSCs is orbital selectivity, as described above. Our effective model incorporates an exchange orbital-anisotropy factor $A_o = J_1^{xy}/J_1^{xz/yz} = J_2^{xy}/J_2^{xz/yz}$, and reflects the orbital selectivity by A_o's deviation from 1. For the iron selenides, A_o is expected to be considerably smaller than 1 (see Supplementary Information).

We are now in a position to discuss how the $s\tau_3$ pairing state emerges in a range of parameters where the s- and d-wave pairing channels are quasi-degenerate. Within the five-orbital t–J_1–J_2 model, we focus on the case with a kinetic part appropriate for the alkaline iron selenides $K_yFe_{2-x}Se_2$, although similar behavior emerges in the cases appropriate for the iron pnictides and single-layer FeSe (see Supplementary Information). We present our results for the case of orbital-diagonal exchange interactions. The inter-orbital exchange interactions have only negligible effects on the pairing amplitudes, as demonstrated in Supplementary Information.

The phase diagram for the alkaline iron selenides is shown in Fig. 2a. In the absence of orbital selectivity, $A_o = 1$, it is known that small and large A_L promote the $s_{x^2y^2} \otimes \tau_0, A_{1g}$ and $d_{x^2-y^2} \otimes \tau_0, B_{1g}$, both defined in the d_{xz}, d_y subspace.[27] Increasing the orbital selectivity, with A_o decreasing from 1, these two limiting regimes remain essentially unchanged. However, in the magnetically frustrated regime $A_L \sim 1$, the $s_{x^2y^2} \otimes \tau_0, A_{1g}$ and $d_{x^2-y^2} \otimes \tau_0, B_{1g}$ become quasi-degenerate. When A_o is sufficiently smaller than 1, the $s\tau_3$ pairing state becomes the dominant channel in the intermediate regime. Similar phase diagrams are obtained for the iron pnictides and single-layer FeSe shown in Fig. 2b and Fig. S1, respectively. A typical dominant $s\tau_3$ pairing case is shown in Fig. S2 and Fig. S1 for a number of subleading symmetry-allowed channels[51] for alkaline iron selenide dispersion with fixed $J_2/J_1 = 1.5$, $A_o = 0.3$, and varying A_L (horizontal axis).

Having established the stability of the $s\tau_3$ pairing state, we now address its salient properties. We first consider the spin-excitation spectrum. In Fig. 3, we show the dynamical spin susceptibility at wavevector $q = (\pi, \pi/2)$ for $J_2 = 1.5$. We note the complicated frequency behavior that can be traced to the anisotropy in the effective gap affecting both the coherence factors and the
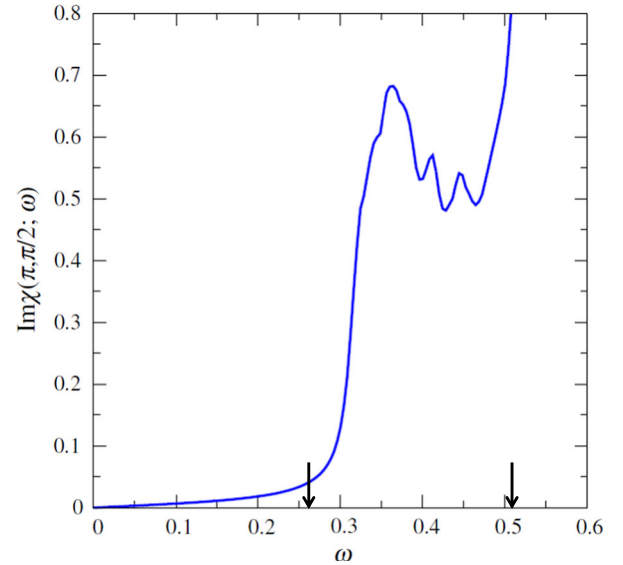

Fig. 3 The imaginary part of the dynamical spin susceptibility for the alkaline iron selenides at wavevector $q = (\pi, \pi/2)$, for a dominant $s\tau_3$ pairing for parameters $J_2 = 1.5$, $A_O = 0.3$, and $A_L = 0.9$. The arrows show twice the minimum and maximum gaps (see Fig. 4b). There is a sharp feature ar $\omega \approx 0.36$ within the bounds of twice the effective gap and below the p–h threshold of roughly 0.41 associated with this wavevector

position of minimum in quasi-particle energy. We show the minimum and maximum particle–hole (p–h) thresholds corresponding to twice the minimum and twice the maximum gaps. As suggested by Fig. 4a and b, states connected by $q = (\pi, \pi/2)$ would correspond to a p–h threshold given roughly by the sum of the minimum and maximum gap. A sharp feature appears below this threshold, confirming the existence of the resonance for $q = (\pi, \pi/2)$ as found in experiments on the alkaline iron selenides.[18, 19, 50] The resonance at this wavevector originates from the sign change of
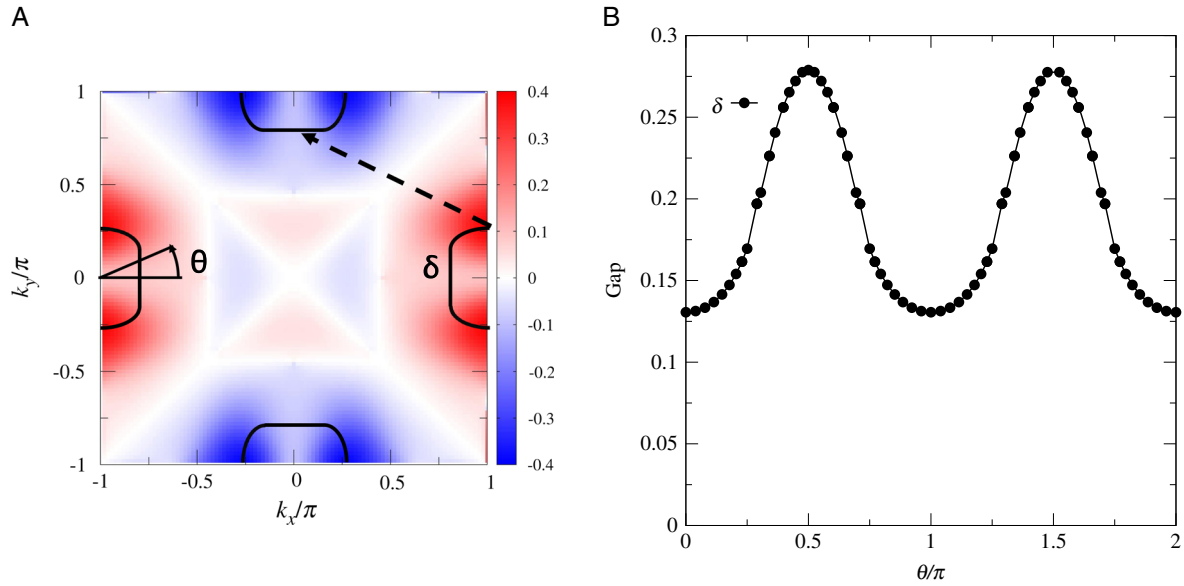
A

B

Fig. 4 **a** The FS (*solid line*) and the real intraband pairing for the band generating the δ pockets at the edge of the BZ for a dispersion typical of the alkaline iron selenides. Note the clear change in sign between pockets separated by the BZ diagonal. The *dashed arrow* indicates the $q = (\pi, \pi/2)$ wavevector associated with the resonance in the spin spectrum found in experiment.[50] **b** The size of the gap along the δ pocket. Both figures are for $J_2 = 1.5$, $A_O = 0.3$, and $A_L = 0.9$ with dominant $s\tau_3$ pairing

the intraband pairing component across the two Fermi pockets at the edge of the BZ, around $(\pm\pi, 0)$ (δ) and $(0, \pm\pi)$, as illustrated in Fig. 4a, and further discussed in Supplementary Information. Without such a sign change, there cannot be a sharp resonance below the p–h threshold energy.

We next turn to the quasiparticle excitation spectrum. Figure 4b shows the gap at the FS as a function of winding angle θ. It clearly illustrates the node-less dispersion, as the gap is nonzero for all θ.

The electron dispersion considered here does not produce any Fermi pockets close to Γ in the BZ. This is in contrast to ARPES experiments on $K_yFe_{2-x}Se_2$,[52, 53] which show a small electron pocket near Γ. Because this electron pocket has very small spectral weight, it is to be expected that even if such a pocket were included, the dominant $s\tau_3$ pairing will still arise; moreover, the gap on this Fermi pocket will be node-less as discussed in the two-orbital case. To substantiate this, we consider the results for the iron pnictides class, which do have significant (albeit hole) Fermi pockets at the zone center yet exhibit a full gap. In Fig. 5a, b, we show the FS and the gaps as functions of winding angle θ for $A_o = 0.5$ and $A_L = 1.3$ corresponding to a dominant $s\tau_3$ pairing. The gap along β is finite and exhibits an anisotropy consistent with the two-orbital results in Eq. 5. In the latter case, at winding angle $\theta = 0$, $\sin\phi = 0$, and the spectrum has a minimum/maximum gap for $E_\pm$. As θ is increased, the $\left|\vec{B}(\mathbf{k}) \times \vec{d}(\mathbf{k})\right|^2$ term increases reaching a maximum at $\theta = \pi/4$. Here the gap is maximum/minimum for $E_\pm$. This is consistent with the anisotropy in the gap shown in Fig. 5.

DISCUSSION

Several remarks are in order. First, the full gap and the sign change of the intraband pairing component discussed above provide evidence that, with strong orbital selectivity, the $s\tau_3$ pairing in a realistic five-orbital model has a behavior very similar to that of the two-orbital case.

Second, with the short-range J_1–J_2 interactions driving superconductivity, pairing involves the electronic states over an extended range of energy about the Fermi energy. The energy window can be determined from the zone-boundary spin-excitation energies, which are on the order of 200 meV for most

iron selenides (and pnictides).[50] This is important for the consideration of the quasiparticle excitation gap at the small electron pocket of $K_yFe_{2-x}Se_2$ near the origin of the BZ. According to the ARPES experiments,[52, 53] this Fermi pocket contains Fe $3d_{xy}$ and Se $4p_z$ orbitals (a band), while the hole (β) bands containing both $3d_{xz}$ and $3d_{yz}$ orbitals are only ~60–80 meV below the Fermi energy. We therefore expect that both the intraband and interband pairing components will be significant for this part of the BZ and the mechanism advanced here will make the quasiparticle excitations to be fully gapped for this small electron pocket.

Third, within our approach, both the iron selenides and pnictides are bad metals in the regime of quasi-degenerate s- and d-wave pairings. However, the iron selenides have stronger correlations, which will lead to a larger ratio of the exchange interaction to renormalized kinetic energy (note that the renormalized bandwidth goes to zero when a bad metal approaches the electron localization transition) and, correspondingly,[27] larger pairing amplitudes. We expect that this will contribute to the larger maximum T_c observed in the iron selenides than in the iron pnictides. Relatedly, the alkaline iron selenides have a stronger orbital selectivity than the iron pnictides, and we thus expect that the $s\tau_3$ pairing is more likely realized in the former than in the latter.

Fourth, it is instructive to compare the mechanism advanced here with a conventional means of relieving quasi-degenerate s- and d-wave pairing states with the trivial orbital structure, which consists in linearly superposing the two into an $s + id$ state. The latter, breaking the time-reversal symmetry, would be stabilized at temperatures sufficiently below the superconducting transition temperature. By contrast, the $s\tau_3$ pairing state preserves the time-reversal symmetry. It is an irreducible representation of the point group, and is therefore stabilized as the temperature is lowered immediately below the superconducting transition. Thus, the emergence of the intermediate $s\tau_3$ pairing state represents a new means to relieve the quasi-degeneracy through the development of orbital selectivity.

Finally, the nodeless d-wave nature of $s\tau_3$ may shed new light on other strongly correlated multi-band superconductors. For instance, one of the striking puzzles emerging in heavy fermion
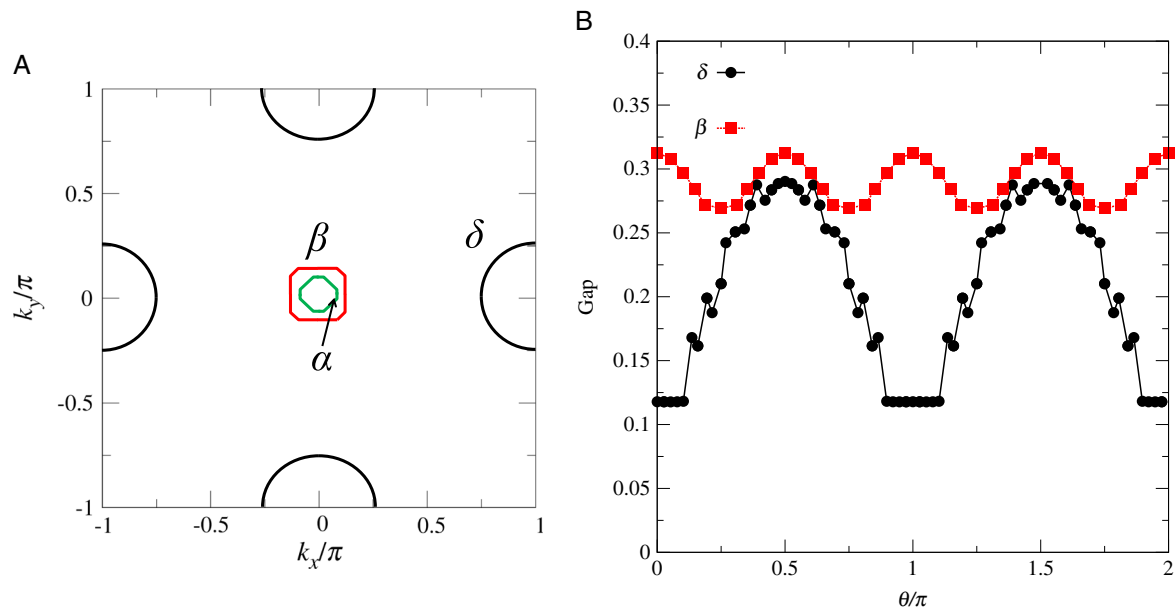
Fig. 5 **a** The FS for the iron pnictides that includes hole pockets around the Γ point with dominant $s\tau_3$, B_{1g} for $J_2 = 1$, $A_L = 1.3$, and $A_O = 0.5$. The tight-binding parameters can be found in ref. 27. **b** The gaps along the β and δ pockets close to the center and edge of the BZ. A similar gap forms around the α pocket

superconductors is the simultaneous exhibition of a variety of *d*-wave characteristics and of a gap in the lowest-energy excitation spectrum.[54] Whether a multiband pairing state such as $s\tau_3$ provides a systematic understanding of such properties is an intriguing open question for future studies.

To summarize, we have demonstrated that an orbital-selective $s\tau_3$ pairing state exhibits properties that would appear mutually exclusive from the conventional perspective, where the orbital degrees of freedom are ignored. It provides a natural understanding of the enigmatic properties observed in the alkaline iron selenides. These include the single-particle excitations, which are fully gapped on the entire FS, as observed in ARPES experiments, and a pairing function, which changes sign across the electron Fermi pockets at the BZ boundary, as indicated by the resonance peak seen near (π, $\pi/2$) in the inelastic neutron scattering experiments. In addition, we have shown that the pairing state is energetically competitive in an orbital-selective model of short-range antiferromagnetic exchange interactions, in the regime where the conventional *s*- and *d*-wave pairing channels are quasi-degenerate. As such, our understanding of the properties of the iron selenide superconductors provides evidence that the high-T_c superconductivity in the iron-based materials originates from the antiferromagnetic correlations of strongly correlated electrons. More generally, our work highlights how new classes of unconventional superconducting pairing state emerge in the presence of additional internal degrees of freedom, with properties that cannot otherwise be expected. This new insight may well be important for the understanding of a variety of other strongly correlated superconductors, including the heavy fermion and organic systems.

METHODS
For a detailed account of our methods, please consult Supplementary Information.

AUTHOR CONTRIBUTIONS
All authors contributed to the research of the work and the writing of the paper.

COMPETING INTERESTS
The authors declare that they have no competing financial interests.

REFERENCES
1. Anderson, P. W. Is there glue in cuprate superconductors? *Science* **316**, 1705–1707 (2007).
2. Kamihara, Y., Watanabe, T., Hirano, M. & Hosono, H. Iron-based layered superconductor La[O$_{1-x}$F$_x$]FeAs (*x*=0.05-0.12) with t$_c$=26 K. *J. Am. Chem. Soc.* **130**, 3296–3297 (2008).
3. Johnston, D. C. The puzzle of high temperature superconductivity in layered iron pnictides and chalcogenides. *Adv. Phys.* **59**, 803–1061 (2010).
4. Si, Q., Yu, R. & Abrahams, E. High-temperature superconductivity in iron pnictides and chalcogenides. *Nat. Rev. Mater.* **1**, 16017 (2016).
5. Wang, F. & Lee, D.-H. The electron-pairing mechanism of iron-based superconductors. *Science* **332**, 200–204 (2011).
6. Hosono, H. & Kuroki, K. Iron-based superconductors: current status of materials and pairing mechanism. *Physica C* **514**, 399–422 (2015).
7. Hirschfeld, P. J. Using gap symmetry and structure to reveal the pairing mechanism in Fe-based superconductors. *C. R. Phys.* **17**, 197–231 (2016).
8. Qazilbash, M. M. et al. Electronic correlations in the iron pnictides. *Nat. Phys.* **5**, 647–650 (2009).
9. Si, Q. & Abrahams, E. Strong correlations and magnetic frustration in the high T_c iron pnictides. *Phys. Rev. Lett.* **101**, 076401 (2008).
10. Yin, Z. P., Haule, K. & Kotliar, G. Magnetism and charge dynamics in iron pnictides. *Nat. Phys.* **7**, 294–297 (2011).
11. Wang, Q.-Y. et al. Interface-induced high-temperature superconductivity in single unit-cell FeSe films on SrTiO₃. *Chin. Phys. Lett.* **29**, 037402 (2012).
12. Lee, J. J. et al. Interfacial mode coupling as the origin of the enhancement of T$_c$ in FeSe films on SrTiO₃. *Nature.* **515**, 245–248 (2014).

13. Mou, D. et al. Distinct fermi surface topology and nodeless superconducting gap in a $(Tl_{0.58}Rb_{0.42})Fe_{1.72}Se_2$ superconductor. *Phys. Rev. Lett.* **106**, 107001 (2011).

14. Zhang, C. et al. Measurement of a double neutron-spin resonance and an anisotropic energy gap for underdoped superconducting $NaFe_{0.985}Co_{0.015}As$ using inelastic neutron scattering. *Phys. Rev. Lett.* **111**, 207002 (2013).

15. Wang, X.-P. et al. Strong nodeless pairing on separate electron Fermi surface sheets in $(Tl, K)Fe_{1.78}Se_2$ probed by ARPES. *Europhys. Lett.* **93**, 57001 (1)–(4). (2011).

16. Xu, M. et al. Evidence for an s-wave superconducting gap in $K_xFe_{2-y}Se_2$ from angle-resolved photoemission. *Phys. Rev. B* **85**, 220504 (2012).

17. Wang, X.-P. et al. Observation of an isotropic superconducting gap at the Brillouin zone center of $Tl_{0.63}K_{0.37}Fe_{1.78}Se_2$. *Europhys. Lett.* **99**, 67001 (2012).

18. Park, J. T. et al. Magnetic resonant mode in the low-energy spin-excitation spectrum of superconducting $Rb_2Fe_4Se_5$ single crystals. *Phys. Rev. Lett.* **107**, 177005 (2011).

19. Friemel, G. et al. Reciprocal-space structure and dispersion of the magnetic resonant mode in the superconducting phase of $Rb_xFe_{2-y}Se_2$ single crystals. *Phys. Rev. B* **85**, 140511(R) (2012).

20. Eschrig, M. The effect of collective spin-1 excitations on electronic spectra in high-T_c superconductors. *Adv. Phys.* **55**, 47–183 (2006).

21. Schaibley, J. R. et al. Valleytronics in 2D materials? *Nat. Rev. Mater.* **1**, 16055 (2016).

22. Yi, M. et al. Observation of universal strong orbital-dependent correlation effects in iron chalcogenides. *Nat. Commun.* **6**, 7777 (2015).

23. Yi, M. et al. Observation of temperature-induced crossover to an orbital-selective Mott phase in $A_xFe_{2-y}Se_2$ (A=K, Rb) superconductors. *Phys. Rev. Lett.* **110**, 067003 (2013).

24. Wang, Z. et al. Orbital-selective metalinsulator transition and gap formation above T_c in superconducting $Rb_{1-x}Fe_{2-y}Se_2$. *Nat. Commun.* **5**, 3202 (2014).

25. Ding, X., Pan, Y., Yang, H. & Wen, H.-H. Strong and nonmonotonic temperature dependence of Hall coefficient in superconducting $K_xFe_{2-y}Se_2$. *Phys. Rev. B* **89**, 224515 (2014).

26. Li, W. et al. Mott behavior in $K_xFe_{2-y}Se_2$ superconductors studied by pump-probe spectroscopy. *Phys. Rev. B* **89**, 134515 (2014).

27. Yu, R., Goswami, P., Si, Q., Nikolic, P. & Zhu, J.-X. Superconductivity at the border of electron localization and itinerancy. *Nat. Commun.* **4**, 2783 (2013).

28. Liu, Z. K. et al. Experimental observation of incoherent-coherent crossover and orbital-dependent band renormalization in iron chalcogenide superconductors. *Phys. Rev. B* **92**, 235138 (2015).

29. Yu, R. & Si, Q. Mott transition in multiorbital models for iron pnictides. *Phys. Rev. B* **84**, 235115 (2011).

30. Yu, R. & Si, Q. Orbital-selective Mott phase in multiorbital models for alkaline iron selenides $K_{1-x}Fe_{2-y}Se_2$. *Phys. Rev. Lett.* **110**, 146402 (2013).

31. de Medici, L., Giovannetti, G. & Capone, M. Selective Mott physics as a key to iron superconductors. *Phys. Rev. Lett.* **112**, 177001 (2014).

32. Yu, R., Zhu, J.-X. & Si, Q. Orbital-selective superconductivity, gap anisotropy, and spin resonance excitations in a multiorbital t–J_1–J_2 model for iron pnictides. *Phys. Rev. B* **89**, 024509 (2014).

33. Yin, Z. P., Haule, K. & Kotliar, G. Spin dynamics and orbital-antiphase pairing symmetry in iron-based superconductors. *Nat. Phys.* **10**, 845–850 (2014).

34. Ong, T., Coleman, P. & Schmalian, J. Concealed d-wave pairs in the $s_\pm$ condensate of iron-based superconductors. *Proc. Natl Acad. Sci. USA* **113**, 5486–5491 (2016).

35. Hao, N. & Hu, J. Odd parity pairing and nodeless antiphase $s_\pm$ in iron-based superconductors. *Phys. Rev. B* **89**, 045144 (2014).

36. Raghu, S., Qi, X.-L., Liu, C.-X., Scalapino, D. J. & Zhang, S.-C. Minimal two-band model of the superconducting iron oxypnictides. *Phys. Rev. B* **77**, 220503(R) (2008).

37. Balian, R. & Werthamer, N. R. Superconductivity with pairs in a relative p wave. *Phys. Rev.* **131**, 1553–1564 (1963).

38. Leggett, A. J. A theoretical description of the new phase of ^{3}He. *Rev. Mod. Phys.* **47**, 331–414 (1975).

39. Sigrist, M. & Ueda, K. Phenomenological theory of unconventional superconductivity. *Rev. Mod. Phys.* **63**, 239–311 (1991).

40. Fang, C., Yao, H., Tsai, W.-F., Hu, J. P. & Kivelson, S. A. Theory of electron nematic order in LaFeAsO. *Phys. Rev. B* **77**, 224509 (2008).

41. Xu, C., Müller, M. & Sachdev, S. Ising and spin orders in the iron-based superconductors. *Phys. Rev. B* **78**, 020501(R) (2008).

42. Seo, K., Bernevig, B. A. & Hu, J. Pairing symmetry in a two-orbital exchange coupling model of oxypnictides. *Phys. Rev. Lett.* **101**, 206404 (2008).

43. Moreo, A., Daghofer, M., Riera, J. A. & Dagotto, E. Properties of a two-orbital model for oxypnictide superconductors: magnetic order, B_{2g} spin-singlet pairing channel, and its nodal structure. *Phys. Rev. B* **79**, 134502 (2009).

44. Chen, W.-Q., Yang, K.-Y., Zhou, Y. & Zhang, F.-C. Strong coupling theory for superconducting iron pnictides. *Phys. Rev. Lett.* **102**, 047006 (2009).

45. Yang, F., Wang, F. & Lee, D.-H. Fermiology, orbital order, orbital fluctuations, and Cooper pairing in iron-based superconductors. *Phys. Rev. B* **88**, 100504(R) (2013).

46. Berg, E., Kivelson, S. A. & Scalapino, D. J. A twisted ladder: relating the Fe superconductors to the high-T_c cuprates. *New J. Phys.* **11**, 085007 (2009).

47. Lv, W., Krüger, F. & Phillips, P. Orbital ordering and unfrustrated $(\pi,0)$ magnetism from degenerate double exchange in the iron pnictides. *Phys. Rev. B* **82**, 045125 (2010).

48. Bascones, E., Valenzuela, B. & Calderón, M. J. Orbital differentiation and the role of orbital ordering in the magnetic state of fe superconductors. *Phys. Rev. B* **86**, 174508 (2012).

49. Graser, S., Maier, T. A., Hirschfeld, P. J. & Scalapino, D. J. Near-degeneracy of several pairing channels in multiorbital models for the Fe pnictides. *New J. Phys.* **11**, 025016 (2009).

50. Dai, P. Antiferromagnetic order and spin dynamics in iron-based superconductors. *Rev. Mod. Phys.* **87**, 855–896 (2015).

51. Goswami, P., Nikolic, P. & Si, Q. Superconductivity in multi-orbital t-J_1-J_2 model and its implications for iron pnictides. *Europhys. Lett.* **91**, 37006 (2010).

52. Zhang, Y. et al. Nodeless superconducting gap in $A_xFe_2Se_2$(A=K, Cs) revealed by angle-resolved photoemission spectroscopy. *Nat. Mater.* **10**, 273–277 (2011).

53. Liu, Z.-H. et al. Three dimensionality and orbital characters of the Fermi surface in $(Tl, Rb)_yFe_{2-x}Se_2$. *Phys. Rev. Lett.* **109**, 037003 (2012).

54. Kittaka, S. et al. Multiband superconductivity in unexpected deficiency of nodal quasiparticles in $CeCu_2Si_2$. *Phys. Rev. Lett.* **112**, 067002 (2014).

55. Nica, E. M., Yu, R. & Si, Q. Glide reflection symmetry, Brillouin zone folding and superconducting pairing for $P4/nmm$ space group. *Phys. Rev. B* **92**, 174520 (2015).